Improving the detection performance of mango firmness using a self-designed pneumatic-electromagnetic-driven impact device with the same impact force control

Kun Tao[1,2,3], Changqing An[1,2,3], Shijie Tian[4], Huirong Xu[1,2,3*]

(1. *College of Biosystems Engineering and Food Science, Zhejiang University, Hangzhou 310058, China*;
2. *Zhejiang Key Laboratory of Intelligent Sensing and Robotics for Agriculture, Hangzhou 310058, China*;
3. *Key Laboratory of on-Site Processing Equipment for Agricultural Products, Ministry of Agriculture and Rural Affairs, Hangzhou 310058, China*;
4. *College of Information Engineering, Northwest A&F University, Yangling 712100, Shaanxi, China*)

Abstract: Mango firmness is one of the critical indicators for assessing internal quality and taste, as well as an indirect measure of maturity and freshness during ripening. Acoustic vibration technology has been widely applied for nondestructive detection of fruit firmness. However, existing detection systems face the risk of fruit damage, prediction performance limitations, and significant influence of fruit size. This study designed a nondestructive pneumatic-electromagnetic-driven impact device based on acoustic vibration technology for firmness detection of different sizes of mango with the same impact force control. Vibration signals of 156 mangoes were acquired using an embedded accelerometer, and effective vibration signals were selected by comparing the excitation vibration response signals and the free vibration response signals. The correlation between mango reference firmness and vibration signal features was then analyzed. Based on this analysis, a prediction model for mango firmness was developed using partial least squares regression based on competitive adaptive reweighted sampling (CARS-PLSR). The results showed that the energy-type and amplitude-type statistical features in the vibration signals had a good correlation with the reference firmness ($|r|\geq0.45$), and the mango firmness prediction model based on the vibration frequency-domain signals (CARS-PLSR) had the optimal performance. The model's prediction determination coefficient (R_P^2), root mean square error of prediction (*RMSEP*), and relative percent deviation (RPD_P) were 0.95, 0.29 N/mm, and 4.20, respectively. Overall, it demonstrated that the pneumatic-electromagnetic-driven impact device integrated with an embedded accelerometer enables accurate and nondestructive detection of mango firmness. The innovative combination of pneumatic control and electromagnetic drive effectively minimizes the impact of fruit size variations and enhances prediction accuracy, demonstrating the significant potential for real-time fruit firmness sorting applications.

Keywords: mango firmness, vibration signal detection, pneumatic-electromagnetic-driven impact device, signal feature extraction, CARS-PLSR

DOI: 10.25165/j.ijabe.20251804.9645

Citation: Tao K, An C Q, Tian S J, Xu H R. Improving the detection performance of mango firmness using a self-designed pneumatic-electromagnetic-driven impact device with the same impact force control. Int J Agric & Biol Eng, 2025; 18(4): 282–292.

1 Introduction

Mango (*Mangifera indica* L.) is rich in nutrients, containing carbohydrates, vitamins, proteins, dietary fiber, and trace elements. However, it is a typical climacteric fruit that will transition from physiological to edible maturity after harvest. The fruit firmness is a reliable indicator for assessing its internal quality[1], as it is significantly related to attributes such as flavor, maturity, shelf life, and sensitivity to mechanical impacts[2]. By detecting firmness, fruit can be classified into different grades or specifications to meet various market demands[3]. Therefore, exploring reliable technologies or methods for detecting mango firmness and grading early in the supply chain is crucial.

Over the years, many studies have explored the rapid and nondestructive technologies or methods to detect the firmness of various fruit, including optical imaging technologies[4], spectral technologies[5–7], electrical properties methods[8–10], micro-deformation methods[11], ultrasound technologies[12], and acoustic vibration technologies[13–17]. Among these technologies and methods, acoustic vibration technology has been recognized as a widely used and efficient technology for detecting the firmness of agricultural products owing to its rapid, nondestructive advantages and stronger correlation with fruit textural attributes[18,19]. The vibration response of fruit depends on its elastic modulus, Poisson's ratio, density, mass, and shape. At the microscopic level, the mechanical and structural properties of fruit depend on the features of its cells (i.e., cell size, cell wall thickness, and turgor pressure) manifest as textural attributes (i.e., crispness, juiciness, firmness, and mealiness).

In previous studies, Fathizadeh et al.[15] used a pendulum impact mechanism combined with a microphone to receive sound signals

Received date: 2024-12-24 **Accepted date:** 2025-05-19

Biographies: Kun Tao, MS candidate, research interest: nondestructive detection of agricultural product quality, Email: tao_kun@zju.edu.cn; **Changqing An**, PhD candidate, research interest: nondestructive detection of agricultural product quality, Email: changqing_an@zju.edu.cn; **Shijie Tian**, PhD, research interest: agricultural internet of things, Email: sjtian@nwafu.edu.cn.

***Corresponding author: Huirong Xu**, Professor, research interest: nondestructive detection technology for internal quality of agricultural products, agricultural intelligent equipment. College of Biosystems Engineering and Food Science, Zhejiang University, 866 Yuhangtang Road, Hangzhou 310058, China. Tel: +86 571 88982282, Email: hrxu@zju.edu.cn.

and a contact accelerometer to receive vibration signals from apples. Results showed that the indicator F_{sum} of acoustic vibration signals was a promising choice for apple firmness detection. However, the results are obtained on apples of approximately the same size, which may cause damage to the fruit. Pourkhak et al.[16] used a linear solenoid actuator to obtain kiwifruits' forced impact signals with load cell and acoustic impulse response with a microphone, integrating multi-sensor data to predict the apparent modulus of elasticity (E_a) and Magness-Taylor firmness (MTf) of kiwifruits. However, this method needs to adjust the height of the impactor according to the size of the samples to ensure that the samples of different sizes receive the same impact force. Zhang et al.[17] developed an acoustic vibration device using three identical piezoelectric sensors in contact with pear samples: one excited the pears (actuator), while the other two detected the pears' vibration response (sensor). Results showed that the resonant frequencies (f_1) from the equator and f_2 from the calyx shoulder of the pear samples were highly correlated with Magness-Taylor firmness (r=0.951). Contact sensors can detect the vibration signals of fruit more stably. However, complex system design may affect the detection efficiency of fruit firmness and easily cause fruit surface damage. In the team's previous study, Tian et al.[20] developed an online detection system for kiwifruit firmness. It utilized an electromagnetic-driven actuator as the excitation device, combined with a microphone sensor to detect the acoustic vibration signals of kiwifruits. However, the microphone sensor is susceptible to interference from environmental noise, and the fruit size influences the impact force of the excitation device. In addition, several commercial devices have been applied to fruit quality detection, such as the Intelligent Firmness Detector[21], Sinclair IQ Firmness Tester[1], and Acoustic Firmness Sensor[22]. These commercial detection devices have achieved rapid and continuous fruit firmness detection to some extent, but still have limitations in detection accuracy. In summary of the above research, the existing detection systems based on acoustic vibration technology face the risk of fruit damage, prediction performance limitations, and significant influence of fruit size.

In this study, a nondestructive pneumatic-electromagnetic-driven impact device for mango firmness detection was designed to reduce the effect of fruit size. The effect of mango firmness characteristics and physical properties on vibration signals was then analyzed, along with the correlation between reference firmness and vibration signal features. Based on this analysis, a regression prediction model for mango firmness was developed using vibration signals.

2 Materials and methods

2.1 Design and construction of the nondestructive detection system

2.1.1 Mango firmness detection system set-up

Based on the previous study[20], a novel pneumatic-electromagnetic-driven impact detection system was designed to detect the vibration of mangoes, as shown in Figure 1. The system consisted of a pneumatic-electromagnetic-driven impact detection device, a static vibration response detection unit, and a data acquisition unit. The impact detection device consisted of an external elastic bellow motion unit, an internal impactor motion unit, and an impactor cover unit. Under air pressure change, the

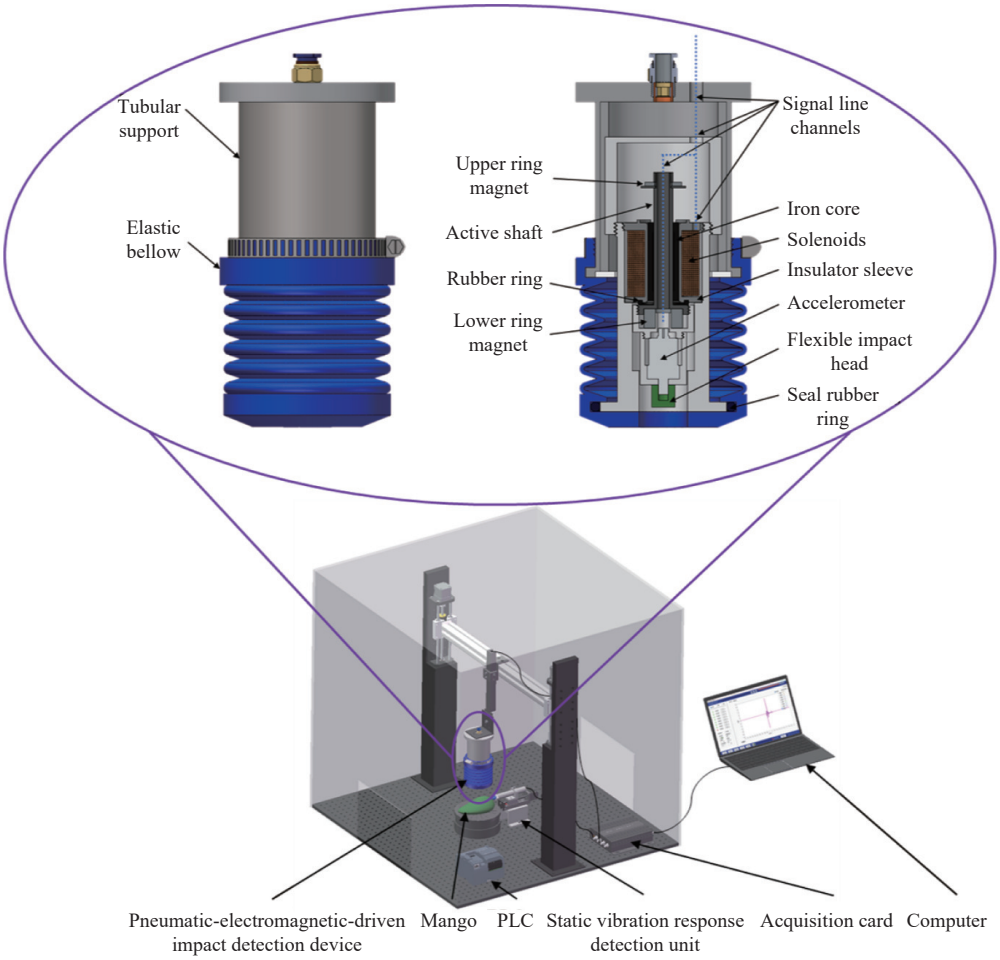

Figure 1 Schematic diagram of mango firmness detection system

elastic bellow could extend and retract with a range of 0-25 mm. The internal impactor motion unit included two ring magnets, an active shaft, an accelerometer, a flexible impact head, and an electromagnet structure formed by an insulation sleeve, solenoids, and an iron core. The ring magnets were neodymium-iron-boron magnets installed at both ends of the active shaft. The interaction between two ring magnets and the electromagnet structure allowed the active shaft to move up and down with the reversal of electric current in the range of 0-20 mm. The flexible impact head was molded and cured from rubber. The accelerometer (YK-YD50, Shanghai Yankun, China) was connected to the flexible impact head, directly detecting the vibration signals of the fruit and transmitting them to the acquisition card (YK-ALM8, Shanghai Yankun, China). The accelerometer had a measurement range of ±50 g, a sensitivity of 100 mV/g, and a frequency range of 0.5-5000 Hz. The sampling rate of the data acquisition card was set to 10 240 Hz, with a sampling duration of 2 s.

In addition, to further analyze and select effective vibration response signals, the detection system was equipped with a static vibration response detection unit, which was used as a vibration pickup device to detect the response characteristics of mango samples under free vibration. The unit consisted of a movable sliding table and an acceleration sensor of the same type as the main system, and the sensor on the sliding table could be close to the surface of the other side of the mango sample to stably collect the free vibration response of the sample.

2.1.2 The procedure of vibration signals detection

As shown in Figure 2, the procedure of mango vibration signal detection was divided into five states. In the initial state, the mango sample was placed on the tray to be detected. In the pre-contact state, the pressurized air started flowing into the detection device through the pneumatic quick connector, and the elastic bellow expanded downwards in the vertical direction, bringing the internal impactor unit close to the surface of the mango sample. In the contact state, the pressurized air continued to flow into the detection device. As the downward expansion of the elastic bellow was obstructed, the internal air pressure increased rapidly. The internal air pressure is monitored by the air pressure sensor to determine that the detection device has been attached to the mango sample. In the acquisition state, the pressurized air stopped flowing into the detection device, and the PLC sent signals to the electromagnet control module for impact detection. In the reset state, the PLC sent signals to the electromagnet control module for impactor reset and to the pneumatic control system to activate the vacuum generator to fast reset the elastic bellow.

The pneumatic control system described mainly includes: air compressor, air supply triplex (air filter, air filter mist, and air regulator), 2-position 3-way solenoid valve, 2-position 2-way solenoid valve, vacuum generator, speed control valve, air pressure sensor and actuator (pneumatic-electromagnetic-driven impact detection device), and its overall configuration and connection are shown in Figure 3. The output pressure of the air regulator in the

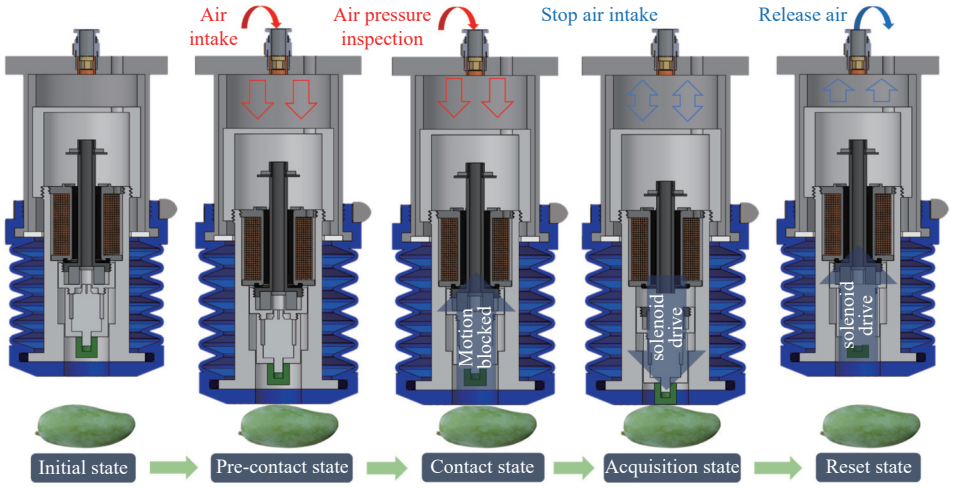

Figure 2 Procedure of mango vibration signals detection

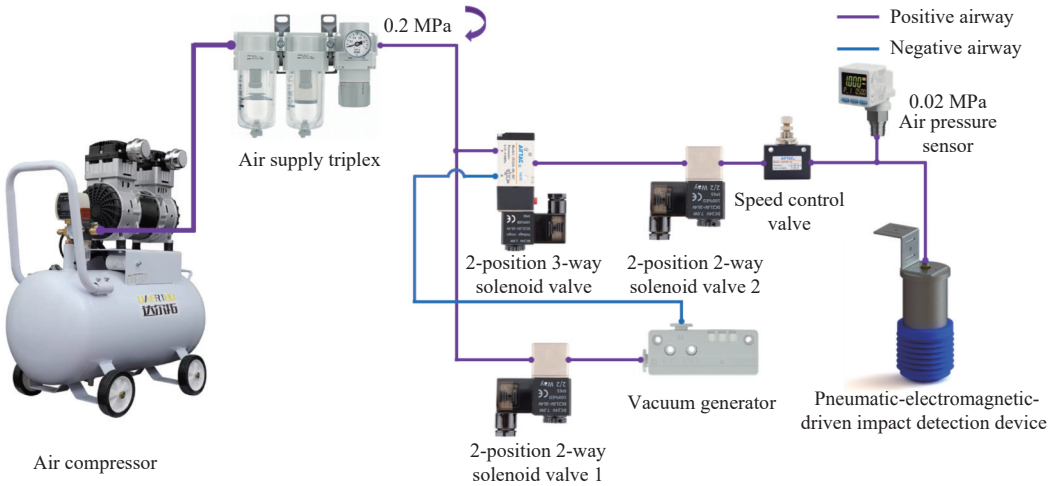

Figure 3 Schematic diagram of pneumatic control system configuration and connection

system is set to 0.2 MPa, the trigger air pressure threshold of the actuator is set to 0.02 MPa, and the opening of the speed control valve is set to 50%.

During the entire procedure of vibration signals detection, pneumatic control enables the bellow to quickly contact the detected mango and controls the internal impactor motion unit to maintain a fixed impact distance from the mango surface, while electromagnetic drive enables the impact detection of the detected mango and controls the constant impact force, which is calibrated to 13.16± 0.12 N. So, the pneumatic-electromagnetic-driven impact device can apply a consistent and stable input to fruits of different sizes.

2.2 Mango samples and measurement process

On April 15, 2024, 120 green mangoes at the green mature stage were purchased, which corresponds to a growth cycle of approximately 120 days after the fruit set. In addition, to enhance the representativeness of the firmness data of the mango samples and to improve the generalizability of the mango firmness prediction model, on November 1, 2024, 36 green mangoes at the full mature stage were purchased, which were matured by the distributor for 2 days after harvesting under hot room conditions with the aid of ethylene. All mango samples were immediately transported to the laboratory after purchase and stored in an artificial climate chamber at 15°C and 80% relative humidity to prevent spoilage.

Six measurements were conducted within two one-week periods to obtain mango samples with different firmness, in which 20 and 6 mango samples were randomly chosen each day for the measurement. Before the measurements, the samples were taken from the artificial climate chamber to recover to room temperature (25°C). Firstly, the weight and size of each mango sample were measured using an electronic balance and caliper, with results recorded in Table 1. Subsequently, vibration signals were detected three times on each side of the cheek for each mango sample. By averaging the six detected signals for each mango sample, 156 vibration signals were obtained. Finally, the reference firmness value of each mango sample was measured using a texture analyzer (TA-XT2i, Stable Micro Systems Ltd., England).

Table 1 Statistics of physical characteristics of mango samples

Physical parameters	Range	Average	Standard deviation
Longitudinal diameter/mm	161.7-235.0	196.5	13.2
Transverse diameter/mm	79.7-125.0	93.9	5.5
Weight/g	511.4-1095.2	741.6	101.3

In the puncture experiment, three measurement points were consistent with the vibration signals detection points on both cheeks of the mango samples. Figure 4a shows the puncture measurement position on the mango. The average of the three values of one cheek represents the firmness of each side of the mango, while the average of the six values represents its overall firmness. During measurement, a cylindrical probe with a diameter of 2 mm was steadily inserted into the unpeeled mango flesh at a speed of 1 mm/s, with a penetration depth of 10 mm[19]. The typical force-displacement curve of the mango is shown in Figure 4b. By analyzing this curve, three relevant firmness indicators can be extracted for puncture initial slope, puncture maximum force, and puncture stabilized mean force, which are characterized as stiffness (S), peel rupture maximum force (F_s), and flesh puncture mean force (F_f), respectively. To determine the best reference of mango firmness, five samples of different maturities were selected from the total mango samples (three stored for two days and two stored for four days) to analyze their force-displacement curves and extract three firmness indicators.

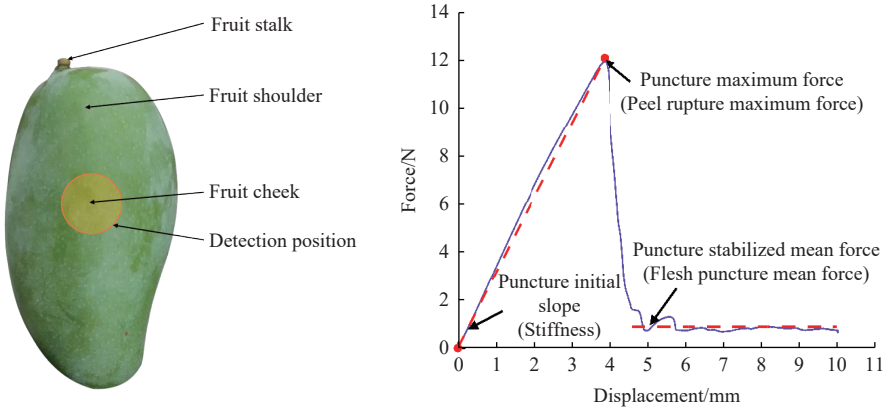

a. Puncture measurement position on the mango b. The force-displacement curve of mango

Figure 4 Mango firmness puncture experiment set-up and results

2.3 Vibration signals composition analysis

The vibration signals were directly transmitted to the accelerometer after the flexible impact head contacted the mango surface. As shown in Figure 5, the detected mango vibration time-domain signal lasted 0.277 s and exhibited a maximum peak. This vibration signal characteristic was similar to the results obtained by other researchers[2,23–24]. Time-domain analysis provided direct observation of the signal shape. The entire signal period could be divided into two phases based on the start moment, the end moment, and the maximum peak moment of the vibration response.

2.4 Feature extraction of mango vibration signals

In the detected mango vibration signals, the time-domain information reflected the variation of the signals over time. The

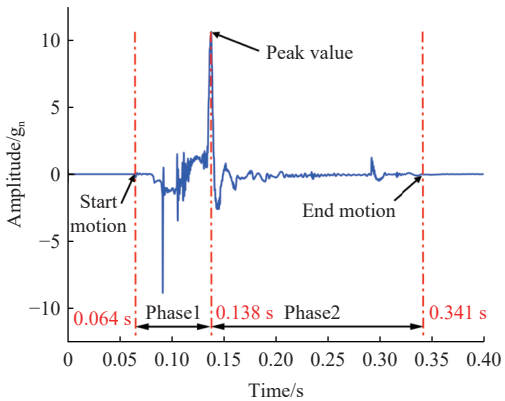

Figure 5 Raw vibration time-domain signal

initial time-domain signals were transformed into frequency-domain signals using the Fast Fourier Transform (FFT) algorithm[25], which reflected the energy distribution of the signals at different frequencies. Vibration signals are often nonstationary, and their frequency components may change over time. The extraction of time and frequency domain features combines the advantages of both domains, providing a more comprehensive signal description. Several statistical features were extracted from the vibration signals in the time and frequency domain, respectively.

In these features, the mean absolute value and root mean square reflect the energy level of the signals; kurtosis reflects the sharpness of the signal waveform; skewness measures the position of the signal peak relative to the mean; variance, max amplitude, and waveform factor all reflect the variability of the signals; peak factor reflects the relationship between the signal peak and the average energy level; impulse factor describes the pulse feature of the signals; margin factor reflects the degree of variation in the signal amplitude; resonant frequency refers to the frequency at which the system produces maximum amplitude response, reflecting the inherent characteristics of the system; half-peak width is the width of the frequency spectrum peak, reflecting the bandwidth of the signals and the damping characteristics of the system; and peak area is related to the energy or power of the signals and can reflect the total energy of the signals within a specific frequency range.

2.5 Data analysis

2.5.1 Correlation analysis

In the firmness measurement of mango, the force-displacement curve was used to obtain the reference firmness. Furthermore, extracting the time and frequency domain features of the mango's vibration signals provided a more comprehensive description of the vibration signals. To analyze the feasibility of mango firmness detection using the detected vibration signals, Pearson correlation analysis was used to assess the correlation between reference firmness and vibration signal features. The formula for the Pearson correlation coefficient is shown in Equation (1), which measures the linear correlation between two variables, with values ranging from −1 to 1.

$$r = \frac{\sum (X-\bar{X})(Y-\bar{Y})}{\sqrt{\sum (X-\bar{X})^2}\sqrt{\sum (Y-\bar{Y})^2}} \quad (1)$$

where, X is the signal feature of the samples, $\bar{X}$ is the mean value of X, Y is the reference firmness value of the samples, and $\bar{Y}$ is the mean value of Y.

2.5.2 Signal denoising methods

In practical detection, the raw vibration signals often contain noise due to environmental interference, equipment issues, and signal distortion, which may introduce sharp jumps or spikes in the raw signals, thereby affecting the accuracy of the analysis results. Thus, preprocessing the raw signals is vital for enhancing the signal-to-noise ratio (SNR) and eliminating interference[26]. In this study, the raw vibration time and frequency domain signals were preprocessed using moving average smoothing (MAS), multivariate scatter correction (MSC)[27], standard normal variate transformation (SNV) [28], and Savitzky-Golay smoothing (SG).

2.5.3 Regression modeling

Partial least squares regression (PLSR) is a multivariate statistical analysis method primarily used to establish a regression model between a dependent variable (response variable) and a set of independent variables (explanatory variables)[29]. PLSR has been shown to effectively handle high-dimensional datasets and address multicollinearity issues in fields such as chemometrics. This study employed the PLSR algorithm to perform regression analysis on both vibration time and frequency domain signals to determine the accuracy of vibration signals in predicting mango firmness. Before modeling, all samples were divided into calibration and prediction sets in a 3:1 ratio based on gradient. During the modeling process, the optimal number of latent variables (LV) was determined using a 5-fold Monte Carlo cross-validation method, with the maximum LV set at 25 to avoid overfitting. The PLSR analysis was performed using MATLAB 2023b.

2.5.4 Feature variable selection methods

The establishment of multivariate calibration models typically includes all detected signals, and such a full-variable model will inevitably contain a lot of redundant information, which may reduce the accuracy and stability of the model[30]. Both experimental and theoretical evidence have demonstrated that using feature variable selection methods can optimize the predictive performance of calibration models. The competitive adaptive reweighted sampling (CARS)[31] algorithm simulates a "biological evolution" process, adaptively reweighting and selecting all variables while gradually eliminating redundant and unimportant variables. This study employed the CARS algorithm to extract feature variables.

2.5.5 Evaluation of models

The predictive capability of different models was compared using the coefficient of determination (R_C^2 and R_P^2) for the calibration set and prediction set, the root mean square error (*RMSEC* and *RMSEP*) for the calibration set and prediction set, and the relative percent deviation (RPD_P) for the prediction set. Generally, higher R^2 and *RPD* values, along with lower *RMSE* values, indicate better prediction model performance. The formulas for the above parameters are as follows:

$$R^2 = 1 - \frac{\sum_{i=1}^{n}(y_i-\hat{y}_i)^2}{\sum_{i=1}^{n}(y_i-\bar{y})^2} \quad (2)$$

$$RMSE = \sqrt{\frac{1}{n}\sum_{i=1}^{n}(y_i-\hat{y}_i)^2} \quad (3)$$

$$RPD = \frac{SD}{RMSE} \quad (4)$$

where, n is the number of samples, y is the reference firmness value, y_i is the reference firmness value in fruit number i, $\bar{y}$ is the mean value of reference firmness, and $\hat{y}_i$ is the firmness value predicted by the model. *SD* represents the standard deviation of the firmness values in the dataset.

3 Results and discussion

3.1 Statistics of firmness of mango samples

The firmness indicators of five mango samples, including stiffness (S), peel rupture maximum force (F_s), and flesh puncture mean force (F_f), were obtained through the puncture experiment. As shown in Figure 6, for the stiffness, the difference between the mean values of the measurements of both cheeks of the mango samples was small, with a mean error of 0.18 N/mm, and the coefficients of variation of the measurements were generally low (CV<15%), which indicated that the indicator had high measurement stability and low dispersion. For the peel rupture maximum force, the difference between the mean values of the

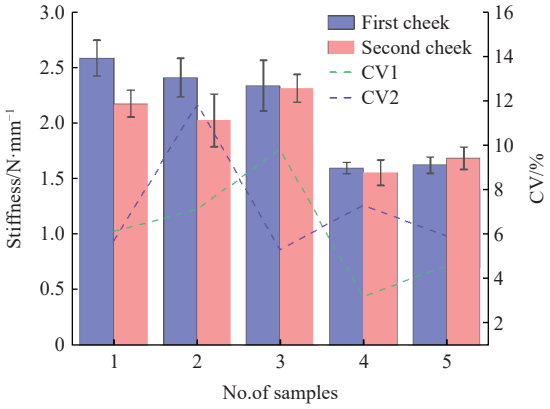

a. Stiffness

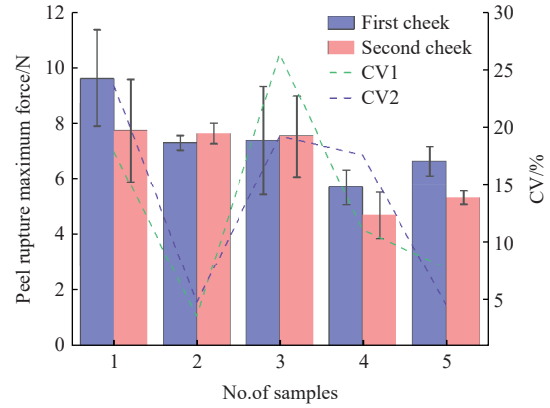

b. Peel rupture maximum force

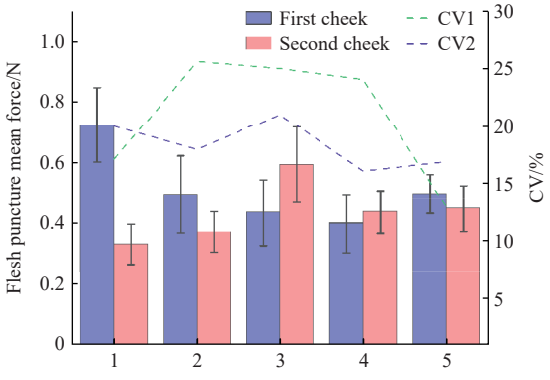

c. Flesh puncture mean force

Figure 6 Statistics of three firmness indicators of five mango samples

measurements of both cheeks of the samples was large, with a mean error of 0.94 N, and the coefficient of variation of some samples appeared to be too large (CV>15%), which indicated that the indicator had a certain degree of volatility and poor repeatability. For the flesh puncture mean force, the difference between the mean values of the measurements of both cheeks of the samples was the smallest, with a mean error of 0.15 N. However, the coefficients of variation of the measurements were generally high, indicating that this indicator has a large overall dispersion, although the differences within individual samples were small. Specifically, for the flesh puncture mean force, the measurement values on both fruit cheeks of the mango samples did not correspond to the actual maturity of the mango samples, further suggesting that the stability of the indicator was low.

According to the analysis, the stiffness indicator demonstrated high precision and repeatability, effectively reflecting the firmness differences among mango samples of different maturity. Therefore, the stiffness was chosen to represent the reference firmness of the mango.

The statistical results of the reference firmness values for 156 mango samples are listed in Table 2. The reference firmness on both sides of the mango samples was close. By averaging the reference firmness values from both cheeks of each sample, the overall reference firmness values were obtained, ranging from 1.97 to 8.76 N/mm. The relatively large range of reference firmness values facilitated the establishment of a robust predictive model.

Table 2 Statistics of reference firmness values of mango samples

Position	Stiffness/N·mm⁻¹		
	Range	Mean	Standard deviation
First cheek	1.92-9.34	3.45	1.32
Second cheek	2.01-8.75	3.52	1.31
Overall	1.97-8.76	3.48	1.30

3.2 Vibration signals analysis

3.2.1 Effective vibration signal selection

The mango vibration signals detected by the nondestructive impact device and the static vibration response detection unit are shown in Figure 7a.

The detection signals from the two piezoelectric accelerometers served as the excitation vibration response signal and the free vibration response signal, respectively. In the excitation vibration response signal, the signal response reached the starting point of the

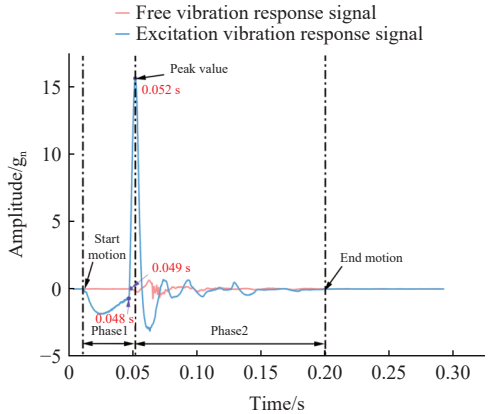

a. Signals detected by nondestructive impact device and static vibration response detection unit

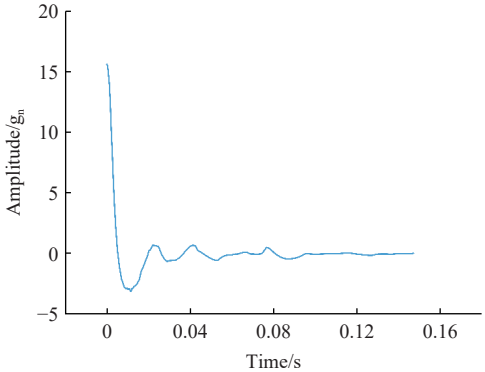

b. Effective vibration signal selected from the raw vibration signal

Figure 7 Signals detected and processed by the nondestructive impact device

peak process at 0.048 s, with a maximum peak occurring at 0.052 s, which decayed and disappeared after approximately 0.200 s. In the free vibration response signal, the signal began to respond after 0.049 s, with the decay disappearing after approximately 0.200 s. By analyzing the timing of the signal response, it could be observed that the second stage of the vibration signal detected by the nondestructive detection device for mango firmness (excitation vibration response signal) almost corresponded to the free vibration signal of the mango sample (free vibration response signal). Therefore, the signal range from the maximum peak moment to the moment the signal decayed and disappeared was selected as the effective vibration signal for the mango sample, as shown in Figure 7b.

3.2.2 Vibration signal analysis of mango samples with different firmness

Figure 8 reveals the vibration time and frequency domain signals of mango samples with different firmness. The softest mango sample had a firmness value of 2.43 N/mm, while the hardest had a firmness value of 8.75 N/mm.

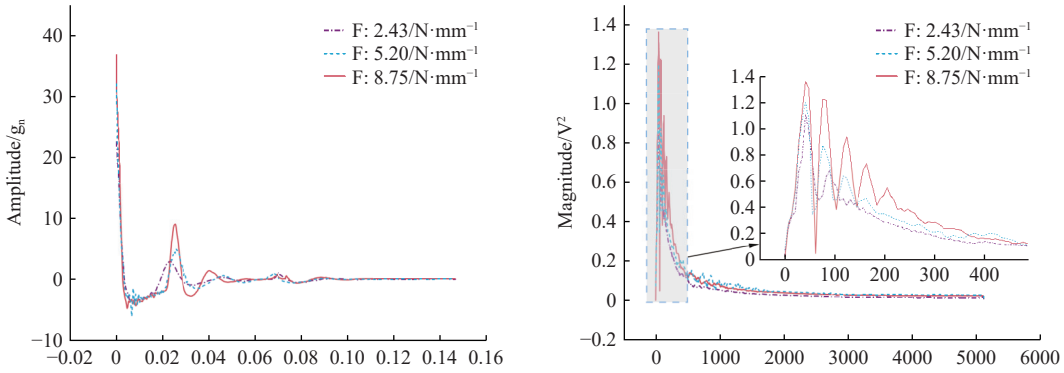

a. Vibration time-domain signals b. Vibration frequency-domain signals

Note: *F* represents the mango firmness (N/mm).

Figure 8 Vibration signals for mango samples with different firmness

In the vibration time-domain signals shown in Figure 8a, as the firmness of the mango samples increased, both the maximum peak and the second peak values of the vibration time-domain signals showed an increasing trend. The maximum peaks of the vibration time-domain signals for the three mango samples were 22.47 g_n (1 g_n=9.806 65 m/s²), 32.20 g_n, and 36.89 g_n, while the second peaks were 2.76 g_n, 4.93 g_n, and 8.97 g_n, respectively. Additionally, as the sample firmness increases from low (2.43 N/mm) to medium (5.20 N/mm), the arrival time point of the second peak of the time-domain signals tends to increase, reflecting the effect of the sample firmness on the vibration decay process. In the vibration frequency-domain signals shown in Figure 8b, as the firmness of the mango samples increased, both the magnitudes of the first resonant peaks and the second resonant peaks exhibited an upward trend. The resonant frequencies also showed a rightward shift. Mangoes with higher firmness value had a tighter cellular structure, enabling them to resist deformation effectively. Thus, higher resonant frequencies and lower damping rates characterized their vibration frequency-domain features.

Overall, the firmness difference of mango samples has a more significant effect on the vibration time and frequency domain signals, and both types of signals can provide rich firmness discriminative information, which provides an effective database for the construction of the mango firmness prediction model.

3.2.3 Vibration signal analysis of mango samples with similar firmness but different sizes

Figure 9 reveals the vibration time and frequency domain signals of mango samples with similar firmness but different sizes.

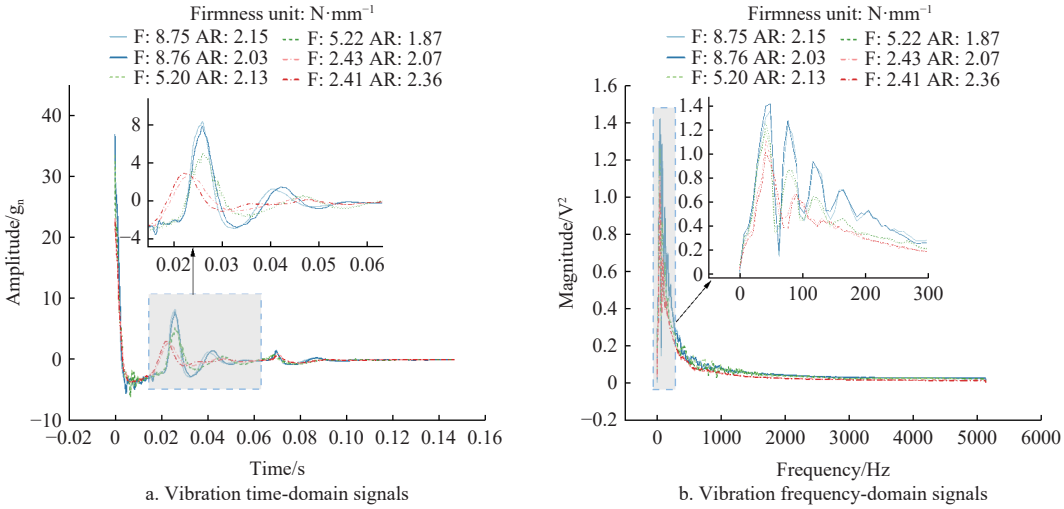

a. Vibration time-domain signals b. Vibration frequency-domain signals

Note: *F* and *AR* represent the mango firmness (N/mm) and aspect ratio, respectively.

Figure 9 Vibration signals for mango samples with similar firmness but different sizes

The six mango samples were divided into three groups, including high firmness (8.75-8.76 N/mm), medium firmness (5.20-5.22 N/mm), and low firmness (2.41-2.43 N/mm), with different fruit sizes and aspect ratios (*AR*=longitudinal diameter/transverse diameter) ranging from 1.87 to 2.36.

In the vibration time-domain signals shown in Figure 9a, the maximum peak values and the second peak values increased with the firmness of the samples, and the time to reach the second peaks also increased with firmness. Although the samples had similar firmness but different fruit sizes in the different firmness groups, the waveforms and amplitudes of the vibration time-domain signals exhibited no significant variations. In the vibration frequency-domain signals shown in Figure 9b, as the firmness of the samples increased, the magnitudes of the first, second, and third resonant peaks all exhibited an upward trend, and the resonant frequencies also showed a rightward shift. Among the different firmness groups, the variations in the magnitude of the first resonant peaks were relatively more significant. In contrast, the variations in the second and third resonant peaks were minor, and the resonant frequency changes were insignificant.

The analysis of vibration time and frequency domain signals from samples with similar firmness but different fruit sizes demonstrated that the pneumatic-electromagnetic-driven impact device designed in this study can effectively reduce the influence of fruit size on vibration signals, ensuring that the detected signal features primarily reflect the firmness of the fruit rather than being significantly affected by the size difference.

3.3 Correlation of vibration signal features with reference firmness

Figure 10 shows the Pearson correlation coefficients between mango reference firmness and the features of its vibration signals in the time and frequency domain.

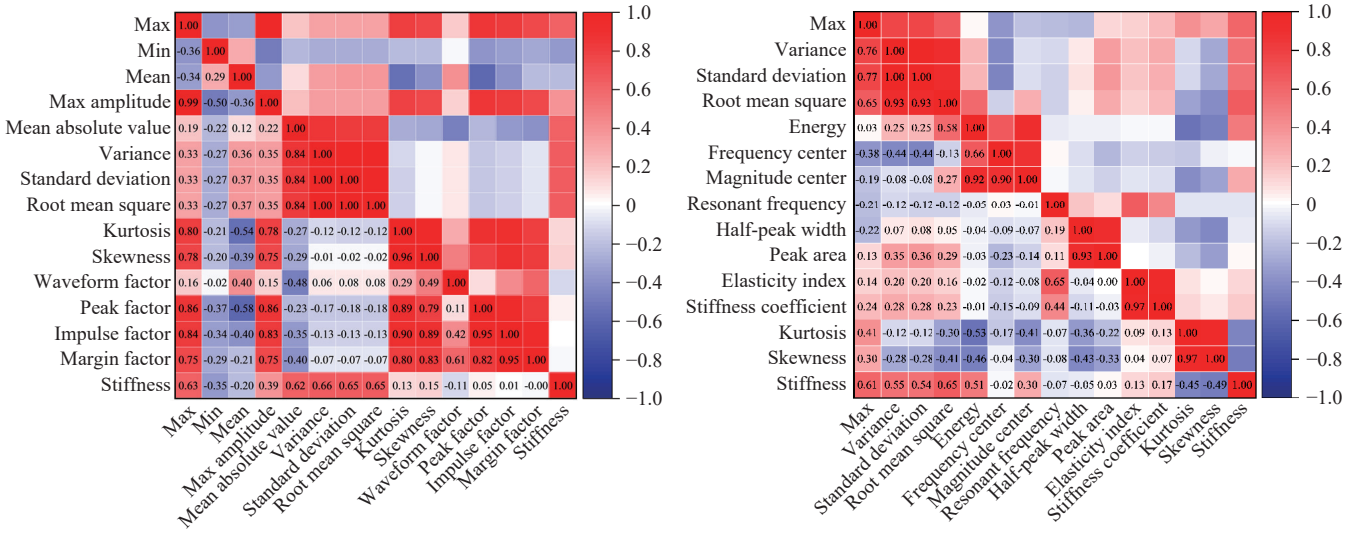

a. Time-domain signal features

b. Frequency-domain signal features

Figure 10 Pearson correlation coefficients between mango firmness and vibration signal features

As shown in Figure 10a, the correlation between reference firmness and vibration time-domain signal features showed that the reference firmness correlated well with the max value, mean absolute value, variance, standard deviation, and root mean square of the vibration time-domain signal features ($|r|\geq0.62$). However, other time-domain features such as kurtosis, skewness, waveform factor, peak factor, impulse factor, and margin factor exhibited weak correlations, reflecting that the energy intensity and volatility features in the time-domain signals were more effective in characterizing mango firmness, while the waveform morphology features were relatively less sensitive to firmness. As shown in Figure 10b, the correlation between reference firmness and vibration frequency-domain signal features indicated that the reference firmness correlated well with the max value, variance, standard deviation, root mean square, energy, kurtosis, and skewness of the vibration frequency-domain signal features ($|r|\geq$ 0.45), reflecting that the energy intensity and frequency structure features of the frequency-domain signals could better reflect the firmness variations of the mango samples.

Overall, the energy-type and amplitude-type statistical features in the mango vibration signals correlate well with the firmness indicator, suggesting that the collected vibration signals have good potential for firmness prediction.

3.4 Mango firmness prediction using PLSR

Table 3 shows the results of the PLSR model combined with different signal preprocessing methods for predicting mango firmness on different full-variable datasets of vibration signals.

Table 3 Results of PLSR models combined with different preprocessing methods in different datasets

Dataset	Preprocess	LV	R_c^2	*RMSEC*/ N·mm^{-1}	R_P^2	*RMSEP*/ N·mm^{-1}	RPD_P
Time-domain signal	Raw	6	0.80	0.57	0.75	0.69	2.04
	MAS	**7**	**0.81**	**0.54**	**0.76**	**0.68**	**2.07**
	MSC	5	0.81	0.55	0.74	0.70	2.03
	SNV	4	0.74	0.65	0.73	0.73	1.95
	SG	4	0.79	0.56	0.74	0.71	1.99
Frequency-domain signal	Raw	6	0.83	0.52	0.77	0.67	2.12
	MAS	**7**	**0.85**	**0.50**	**0.78**	**0.66**	**2.16**
	MSC	5	0.82	0.54	0.76	0.68	2.07
	SNV	4	0.74	0.64	0.66	0.81	1.75
	SG	4	0.78	0.59	0.71	0.75	1.88

In the vibration time-domain signal modeling, the R_P^2, *RMSEP*, and RPD_P of the prediction model based on the raw time-domain signals were 0.75, 0.69 N/mm, and 2.04, respectively. The use of preprocessing methods MSC, SNV, and SG did not significantly improve the model performance, while the MAS preprocessing method performed the best. The R_P^2, *RMSEP*, and RPD_P of the prediction model based on the MAS preprocessed time-domain

signals were 0.76, 0.68 N/mm, and 2.07, respectively. In the vibration frequency-domain signal modeling, the R_P^2, *RMSEP*, and RPD_P of the prediction model based on the raw frequency-domain signals were 0.77, 0.67 N/mm, and 2.12, respectively. Similar to the modeling results based on the time-domain signals, the prediction model based on the MAS preprocessed frequency-domain signals performed optimally, with the R_P^2, *RMSEP*, and RPD_P of 0.78, 0.66 N/mm, and 2.16, respectively.

Overall, MAS preprocessing can provide a certain magnitude of performance improvement in both time and frequency domain signal modeling compared to the original signals, with an average SNR improvement of 19.65 dB and 22.09 dB for all time and frequency domain signals, respectively. This is mainly due to its suppression of random noise, which can reduce the interference of redundant information between variables and enhance the trend interpretability and modeling robustness of the signals.

3.5 Feature variable selection and validation

The results in the previous section indicated that the PLSR mango firmness prediction models based on the vibration signals after MAS preprocessing had better performance. On this basis, to further improve the model performance, the CARS algorithm was used to optimize the feature variables of the preprocessed vibration signals, and the CARS-PLSR mango firmness prediction models based on the selected feature variables were constructed.

As shown in Figures 11a and 11b, the CARS algorithm selected the feature variables that were highly correlated with the firmness of the mango samples from the vibration time-domain signals and the frequency-domain signals, respectively. Among them, the number of selected variables from the time-domain signals was 132, which were mainly distributed near the minimum wave valley and the second wave peak of the signals, and the number of selected variables from the frequency-domain signals was 82, which were mainly distributed near the second resonance peak and the third resonance peak of the signals. The selected time-domain signal and frequency-domain signal feature variables were then used as inputs to build the PLSR mango firmness prediction models, respectively.

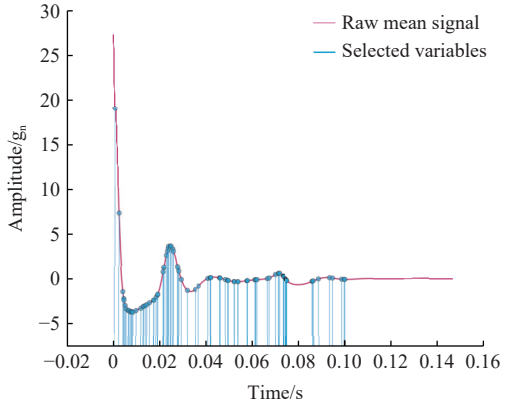

a. Feature variables selected from vibration time-domain signals

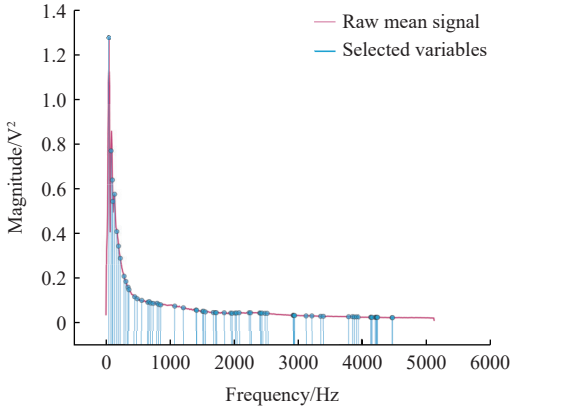

b. Feature variables selected from vibration frequency-domain signals

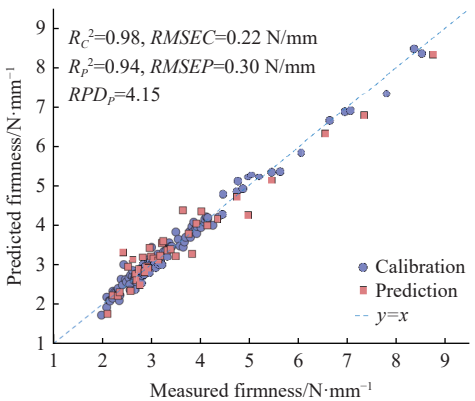

c. Firmness prediction results of vibration time-domain signal dataset

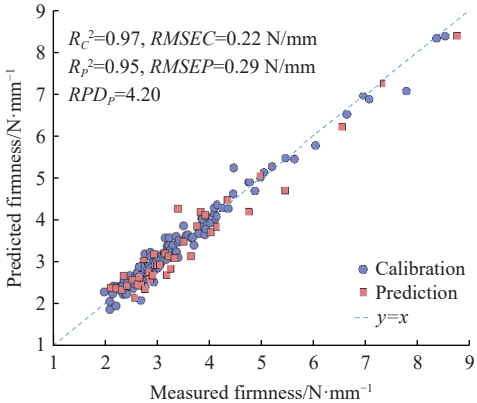

d. Firmness prediction results of vibration frequency-domain signal dataset

Figure 11 Feature variable selection and prediction results by CARS-PLSR model

As shown in Figures 11c and 11d, in the vibration time-domain signal modeling, the R_C^2 and *RMSEC* of the prediction model were 0.98 and 0.22 N/mm, respectively, and the R_P^2, *RMSEP*, and RPD_P were 0.94, 0.30 N/mm, and 4.15, respectively. Compared with the PLSR model based on the full variables of vibration time-domain signals, R_P^2 was improved by 0.18, *RMSEP* was reduced by 0.38 N/mm, and RPD_P was improved by 2.08. In the vibration frequency-domain signal modeling, the R_C^2 and *RMSEC* of the prediction model were 0.97 and 0.22 N/mm, respectively, and the R_P^2, *RMSEP*, and RPD_P were 0.95, 0.29 N/mm, and 4.20, respectively. Compared with the PLSR model based on the full variables of vibration frequency-domain signals, R_P^2 was improved by 0.17, *RMSEP* was reduced by 0.37 N/mm, and RPD_P was improved by 2.04.

The results show that the CARS algorithm can effectively eliminate redundant variables and noise information, retain the feature variables that are highly correlated with the firmness of mango, improve the prediction accuracy and robustness of the models, as well as reduce the input dimension, which is helpful for the rapid deployment of the model and practical application.

Comparing the results of fruit firmness detection in this study with the data published in the literature using acoustic vibration detection technology, the best result (R_P^2=0.95) obtained for mango firmness in this study was similar to the result (R_P^2=0.951) for peach reported by Chen et al.[32], and was slightly lower than the result

(R_P^2=0.956) for kiwifruit reported by Nouri et al.[2]. However, it was higher than the result (R_P^2=0.841) for kiwifruit reported by Pourkhak et al.[16], the result (r_P=0.951) for pear reported by Zhang et al.[17], and the result (r_P=0.832) for pear reported by Ding et al.[33]. In summary, these comparisons demonstrate that high-precision prediction of mango firmness can be achieved using vibration signals collected by the pneumatic-electromagnetic-driven impact device, in combination with the CARS-PLSR modeling approach.

4 Conclusions

This study designed a nondestructive pneumatic-electromagnetic-driven impact device based on acoustic vibration technology for fruit firmness detection with the same impact force control for different-sized fruit. The innovative combination of pneumatic control and electromagnetic drive for the impact device with an embedded accelerometer can effectively address the influence of fruit size and improve prediction performance.

This study collected the vibration response signals and reference firmness values of 156 green mangoes at different storage periods, and effective vibration signals were subsequently selected. The correlation between mango reference firmness and vibration signal features was then analyzed. Based on this analysis, a prediction model for mango firmness was developed using CARS-PLSR. The results indicated that the mango firmness prediction model based on the vibration frequency-domain signals had the optimal performance, and the R_P^2, $RMSEP$, and the RPD_P of the model were 0.95, 0.29 N/mm, and 4.20, respectively.

In summary, the detection device designed in this study demonstrated high accuracy in predicting mango firmness, providing technical support for the quality detection and sorting of postharvest mangoes. Future research directions include further optimizing the detection device and applying this technology to other fruits, aiming to advance the application of acoustic vibration technology in the nondestructive detection of fruit quality.

Acknowledgements

The authors gratefully acknowledge the financial support provided by the National Key R&D Program of China (Grant No. 2022YFD2002201) and the High-Level Talents Special Support Program of Zhejiang province (Grant No. 2023R5250).

[References]

[1] Goldberg T, Agra H, Ben-Arie R. Non-destructive measurement of fruit firmness to predict the shelf-life of ‘Hayward’ kiwifruit. Scientia Horticulturae, 2019; 244: 339–342.

[2] Nouri S F, Abdanan Mehdizadeh S A. Design, construction and evaluation of a device for non-destructive measurement of firmness in fruits using vibration analysis (case study: Kiwifruit). Scientia Horticulturae, 2024; 328: 112965.

[3] Sneddon T, Rivera S, Li M, Heyes J, East A. Non-destructive firmness assessment of ‘SunGold’ kiwifruit a three-year study. New Zealand Journal of Crop and Horticultural Science, 2024; 52(3): 195–209.

[4] Rungpichayapichet P, Nagle M, Yuwanbun P, Khuwijitjaru P, Mahayothee B, Müller J. Prediction mapping of physicochemical properties in mango by hyperspectral imaging. Biosystems Engineering, 2017; 159: 109–120.

[5] Li J B, Zhang H L, Zhan B S, Zhang Y F, Li R L, Li J B. Nondestructive firmness measurement of the multiple cultivars of pears by Vis-NIR spectroscopy coupled with multivariate calibration analysis and MC-UVE-SPA method. Infrared Physics & Technology, 2020; 104: 103154.

[6] Nascimento P A M, Carvalho L C D, Júnior L C C, Pereira F M V, de Almeida Teixeira G H. Robust PLS models for soluble solids content and firmness determination in low chilling peach using near-infrared spectroscopy (NIR). Postharvest Biology and Technology, 2016; 111: 345–351.

[7] Rungpichayapichet P, Chaiyarattanachote N, Khuwijitjaru P, Nakagawa K, Nagle M, Müller J, et al. Comparison of near-infrared spectroscopy and hyperspectral imaging for internal quality determination of ‘Nam Dok Mai’ mango during ripening. Journal of Food Measurement and Characterization, 2023; 17: 1501–1514.

[8] Bhosale A A, Sundaram K K. Firmness prediction of the apple using capacitance measurement. Procedia Technol, 2014; 12: 163–167.

[9] Bian H, Tu P, Hua‐li X, Shi P. Quality predictions for bruised apples based on dielectric properties. Journal of Food Processing and Preservation, 2019; 43(8): e14006.

[10] Fazayeli A, Kamgar S, Nassiri S M, Fazayeli H, de la Guardia M. Dielectric spectroscopy as a potential technique for prediction of kiwifruit quality indices during storage. Information Processing in Agriculture, 2019; 6(4): 479–486.

[11] McGlone V A, Jordan R B. Kiwifruit and apricot firmness measurement by the non-contact laser air-puff method. Postharvest Biology and Technology, 2000; 19(1): 47–54.

[12] Kim K-B, Lee S, Kim M-S, Cho B-K. Determination of apple firmness by nondestructive ultrasonic measurement. Postharvest Biology and Technology, 2009; 52(1): 44–48.

[13] Arai N, Miyake M, Yamamoto K, Kajiwara I, Hosoya N. Soft mango firmness assessment based on Rayleigh waves generated by a laser-induced plasma shock wave technique. Foods, 2021; 10(2): 323.

[14] Ding C Q, Feng Z, Wang D C, Cui D, Li W H. Acoustic vibration technology: Toward a promising fruit quality detection method. Comprehensive Reviews in Food Science and Food Safety, 2021; 20(2): 1655–1680.

[15] Fathizadeh Z, Aboonajmi M, Beygi S R H. Nondestructive firmness prediction of apple fruit using acoustic vibration response. Scientia Horticulturae, 2020; 262: 109073.

[16] Pourkhak B, Mireei S A, Sadeghi M, Hemmat A. Multi-sensor data fusion in the nondestructive measurement of kiwifruit texture. Measurement, 2017; 101: 157–165.

[17] Zhang H, Wu J, Zhao Z Q, Wang Z P. Nondestructive firmness measurement of differently shaped pears with a dual-frequency index based on acoustic vibration. Postharvest Biology and Technology, 2018; 138: 11–18.

[18] Zhang W, Lv Z Z, Xiong S L. Nondestructive quality evaluation of agro-products using acoustic vibration methods-A review. Critical Reviews in Food Science and Nutrition, 2018; 58(14): 2386–2397.

[19] Aboonajmi M, Jahangiri M, Hassan-Beygi S R. A review on application of acoustic analysis in quality evaluation of agro-food products. Journal of Food Processing and Preservation, 2015; 39(6): 3175–3188.

[20] Tian S J, Wang J P, Xu H R. Firmness measurement of kiwifruit using a self-designed device based on acoustic vibration technology. Postharvest Biology and Technology, 2022; 187: 111851.

[21] Blanke M M. Non-invasive assessment of firmness and NIR sugar (TSS) measurement in apple, pear and kiwi fruit. Erwerbs-Obstbau, 2013; 55: 19–24.

[22] Feng J, Wohlers M, Olsson S R, White A, McGlone V A, Seelye R J, et al. Comparison between an acoustic firmness sensor and a near-infrared spectrometer in segregation of kiwifruit for storage potential. XXIX International Horticultural Congress on Horticulture: Sustaining Lives, Livelihoods and Landscapes (IHC2014): 1119, 2014. doi: 10.17660/ActaHortic.2016.1119.39.

[23] Blanes C, Ortiz C, Mellado M, Beltrán P. Assessment of eggplant firmness with accelerometers on a pneumatic robot gripper. Computers and Electronics in Agriculture, 2015; 113: 44–50.

[24] Cortés V, Blanes C, Blasco J, Ortíz C, Aleixos N, Mellado M, et al. Integration of simultaneous tactile sensing and visible and near-infrared reflectance spectroscopy in a robot gripper for mango quality assessment. Biosystems Engineering, 2017; 162: 112–123.

[25] Lin H-C, Ye Y-C. Reviews of bearing vibration measurement using fast Fourier transform and enhanced fast Fourier transform algorithms. Advances in Mechanical Engineering, 2019; 2019(1). doi: 10.1177/1687814018816751.

[26] Khaled A Y, Ekramirad N, Parrish C A, Eberhart P S, Doyle L E, Donohue K D, et al. Non-destructive detection of codling moth infestation in apples using acoustic impulse response signals. Biosystems Engineering, 2022; 224: 68–79.

[27] Mou Y, You X, Xu D Q, Zhou L, Zeng W, Yu S J. Regularized

multivariate scatter correction. Chemometrics and Intelligent Laboratory Systems, 2014; 132: 168–174.

[28] Chi K P, Lin J R, Chen M, Chen J J, Chen Y M, Pan T. Changeable moving window-standard normal variable transformation for Visible-NIR spectroscopic analyses. Spectrochimica Acta Part A: Molecular and Biomolecular Spectroscopy, 2024; 308: 123726.

[29] Wold S, Sjöström M, Eriksson L. PLS-regression: A basic tool of chemometrics. Chemometrics and Intelligent Laboratory Systems, 2001; 58(2): 109–130.

[30] Liu K, Chen X J, Li L M, Chen H L, Ruan X K, Liu W B. A consensus successive projections algorithm – multiple linear regression method for analyzing near infrared spectra. Analytica Chimica Acta, 2015; 858: 16–23.

[31] Li H D, Liang Y Z, Xu Q S, Cao D S. Key wavelengths screening using competitive adaptive reweighted sampling method for multivariate calibration. Analytica Chimica Acta, 2009; 648: 77–84.

[32] Chen N, Liu Z, Zhang T Y, Lai Q R, Zhang J S, Wei X L, et al. Research on prediction of yellow flesh peach firmness using a novel acoustic real-time detection device and Vis/NIR technology. LWT, 2024; 209: 116772.

[33] Ding C Q, Wu H L, Feng Z, Wang D C, Li W H, et al. Online assessment of pear firmness by acoustic vibration analysis. Postharvest Biology and Technology, 2020; 160: 111042.